Hindawi Publishing Corporation
Modelling and Simulation in Engineering
Volume 2012, Article ID 468029, 11 pages
doi:10.1155/2012/468029

Research Article

Prediction of Ship Unsteady Maneuvering in Calm Water by a Fully Nonlinear Ship Motion Model

Ray-Qing Lin, Tim Smith, and Michael Hughes

Hydromechanics Department, David Taylor Model Basin, NSWCCD, 9500 MacArthur Boulevard, West Bethesda, MD 20817-5700, USA

Correspondence should be addressed to Ray-Qing Lin, ray.lin@navy.mil

Received 25 August 2011; Accepted 5 December 2011

Academic Editor: Ahmed Rachid

This is the continuation of our research on development of a fully nonlinear, dynamically consistent, numerical ship motion model (DiSSEL). In this study we will report our results in predicting ship motions in unsteady maneuvering in calm water. During the unsteady maneuvering, both the rudder angle, and ship forward speed vary with time. Therefore, not only surge, sway, and yaw motions occur, but roll, pitch and heave motions will also occur even in calm water as heel, trim, and sinkage, respectively. When the rudder angles and ship forward speed vary rapidly with time, the six degrees-of-freedom ship motions and their interactions become strong. To accurately predict the six degrees-of-freedom ship motions in unsteady maneuvering, a universal method for arbitrary ship hull requires physics-based fully-nonlinear models for ship motion and for rudder forces and moments. The numerical simulations will be benchmarked by experimental data of the Pre-Contract DDG51 design and an Experimental Hull Form. The benchmarking shows a good agreement between numerical simulations by the enhancement DiSSEL and experimental data. No empirical parameterization is used, except for the influence of the propeller slipstream on the rudder, which is included using a flow acceleration factor.

1. Introduction

To predict ship motions in unsteady state maneuvering in calm water, due to both the time-varying angle and ship forward speed, all six degrees-of- freedom ship motions must be considered. Particulary, when the rudder angles and ship forward speed vary rapidly with time, the six degrees-of-freedom of ship motions and interactions between different modes of motion, as well as between rudder and ship body, become strong. A fully nonlinear method to predict the six-degree freedom of ship motions is need.

With the increase in computer capabilities and the development of advanced computation flow prediction methods, the use of numerical methods to predict the steering capabilities of ships has become possible. For example, Lin et al. [1] and Lin and Kuang [2] predicted ship motions in steady turning circles in calm water and seawater by a fully nonlinear hybrid flow ship motion model. Chau [3] and El Moctar [4] used viscous flow methods to predict the rudder flow and Lee [5], Tamashima et al. [6], Han et al. [7], Kinnas et al. [8], and Hacket et al. [9] used potential flow panel methods to compute the rudder force and moment. Notably, Kinnas et al. [8] used a finite element boundary condition to improve the panel method. Recently, Hochbaum et al. summarized the researches on predicting ship motions when ship maneuvering in 25th ITTC conference [10]. Many of them are focused on maneuvering in calm water, especially those unsteady maneuvering. These works have significantly improved the physical understanding of rudder forces and moments. However, as Söding [11] pointed out, those potential flow methods did not take into account viscosity, turbulence, and flow separation. Viscous flow methods for prediction of a ship's steering capabilities still remain technically difficult and computationally expensive. Therefore, in spite of the limitations of potential flow, most practical flow problems are still solved either by experimental data or by potential flow calculations [11].

The current numerical prediction ability cannot satisfy the ship industry's development needs. Most prediction methods are still focused on using observed or empirical

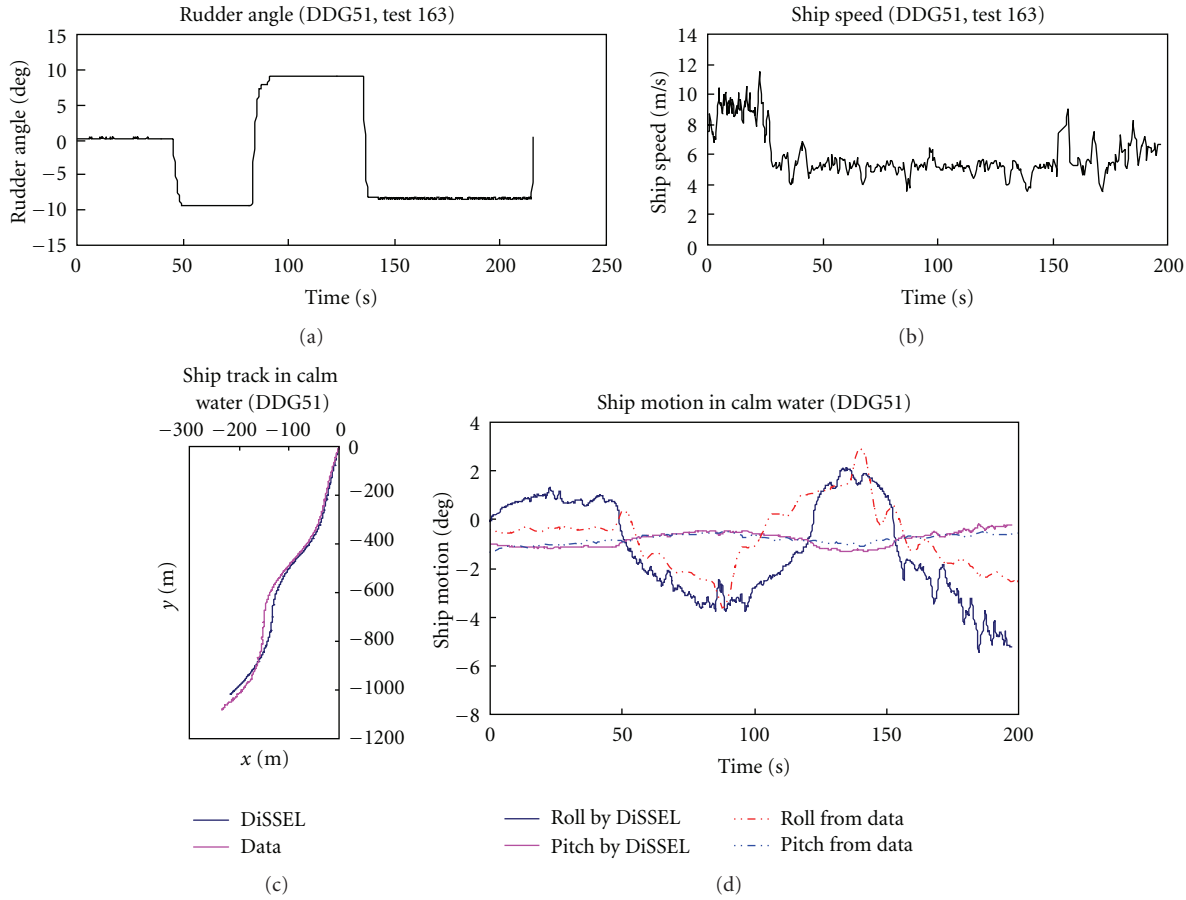

Figure 1: Input data for case 1 are shown in (a) and (b). (a) Rudder angle from data in test 163, (b) ship speed from data in test 163. Benchmark simulations for case 1 are shown in (c) and (d). (c) Comparison of ship tracks between simulation and experimental data in test 163, (d) Comparison of roll and pitch motions between simulations and data in test163.

forces and moments on the rudder for steady or unsteady turning circles. The ship motions often focus on surge, sway, and yaw motions which are calculated by empirical formulations. For example, Altosloe et al. [12], Kimoto et al. [13], and Katayama et al. [14, 15] are popular in ship industry because these methods are accurate even for a planing craft in calm water.

Even though these methods are accurate, they are not appropriate for new and unconventional ships, for which empirical data are not available. Therefore, in [1, 2], a physics-based method was described for the prediction of forces and moments on the rudder for steady turning in calm water and in seaway. When this new method is coupled with a nonlinear six degrees-of-freedom ship motion model (Digital, Self-consistent Ship Experimental Laboratory, we may simply call DiSSEL), the associated surge, sway, and yaw can be accurately predicted. The goal in this study is continue developing a fully nonlinear coupled computational system to accurately predict the ship motion for an unsteady maneuvering ship. Even in calm water, due to the time-varying ship forward speed and rudder angle, the six degrees-of-freedom ship motions as well as their interactions (between different modes of ship motion as well as between the rudder and ship body) all become significant. Therefore, such simulations require a physics-based, fully nonlinear method.

As an example of a fully nonlinear method, the waterline should be defined by local free surface elevation (ship waves and their interactions); the ship position is determined by the six degrees-of-freedom ship motion; the ship motions are determined by the force and moment on the wetted surfaces of the ship hull and of the rudders, and the force and moment are determined by ship and rudder positions, and so forth. Unfortunately, as a propeller model has not yet been implemented in DiSSEL, the influence of the propeller slipstream on the rudder is included empirically by modifying the effective inflow velocity into the rudder to account for the acceleration of the flow by the propeller.

In the following section, a coupled, fully nonlinear rudder force with fully nonlinear ship motion model is presented. Section 3 benchmarks the numerical simulation with experimental data for two ship hulls: Pre-Contract DDG-51 (Model 5514) and Experimental Hull Form. Conclusions are provided in Section 4.

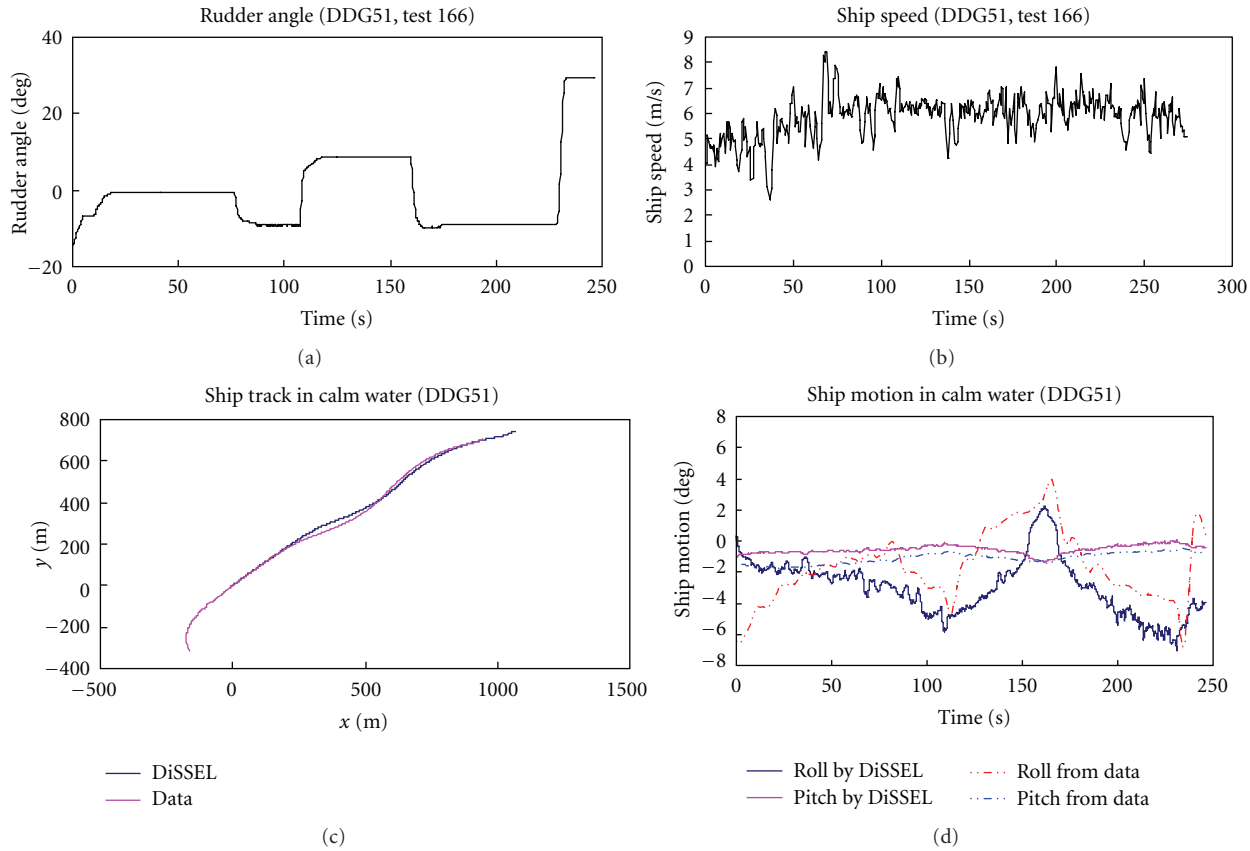

FIGURE 2: Data input for case 2 are shown in (a) and (b). (a) Rudder angle from data in test 166, (b) ship speed from data in test 166. Benchmark simulations for case 2 are shown in (c) and (d). (c) Comparison of ship track between simulation and experimental data in test 166. (d) Comparison of roll and pitch motions between simulations and data in test 166.

2. A Fully Nonlinear Prediction System of Steering Capabilities and Ship Motion Model

DiSSEL is a hybrid-flow ship motion model in time domain: the surface waves are described by velocity potential, but the fluid viscous effect is included in the form of wave breaking and separation effects (Lin et al. [1], and Lin and Kuang [2, 16]). Inclusion of the viscous, separation effect makes DiSSEL satisfying the Kutta condition at a trailing edge, and velocity stagnation points ($\mathbf{V} = 0$), thus allowing accurate evaluation of the lift force (Lin et al. [1]; Lin and Kuang [2]). This hybrid-flow approach builds a solid foundation of our effort to expand the model for ship maneuvering in a seaway.

The fully nonlinear prediction system includes two components. The first component is prediction of rudder forces and moments and the second component is the DiSSEL ship motion model. Before describing the two components, we will overview the method to accurately predict flow separation affect in potential flow theory which was proposed by Lin and Kuang [16].

2.1. "Blocking Theory" in Potential Flow. Landau and Lifshitz [17] pointed out that flow passing an object causes its total pressure to change. However, according to potential flow theory, its total pressure does not change. To correctly calculate the net pressure on the rudder is the key issue for accurately predicting the steering capability. Lin and Kuang [16] proposed a "blocking theory" and suggested total lost pressure due to the separation on the object can be obtained by integrating the pressure over "the affect area" in potential flow. The "affect area" may be referred to as blocking area or separated area. When flow passes an object, without viscosity and turbulence, the pressure is $P_{(s)}$. When viscosity and turbulence are present, the pressure $P_{(s)}$ will change to $P'_{(s)}$ on the object surface, and $P'_{(s)} < P_{(s)}$. This is the separation effect. If Ar is the surface area of the object, then the total hydrodynamic force on the object is

$$\int_{\mathrm{Ar}} \mathbf{n} P'_{(s)} ds, \tag{1}$$

where $\mathbf{n}$ is normal vector of the object. For a potential flow, $P_{(s)}$ is calculated instead of $P'_{(s)}$. In order to obtain the total pressure accurately, one can reduce the object surface area from Ar to Ar−Ae. Then the total hydrodynamic force on the object will be:

$$\int_{\mathrm{Ar-Ae}} \mathbf{n} P_{(s)} ds \approx \int_{\mathrm{Ar}} \mathbf{n} P'_{(s)} ds; \tag{2}$$

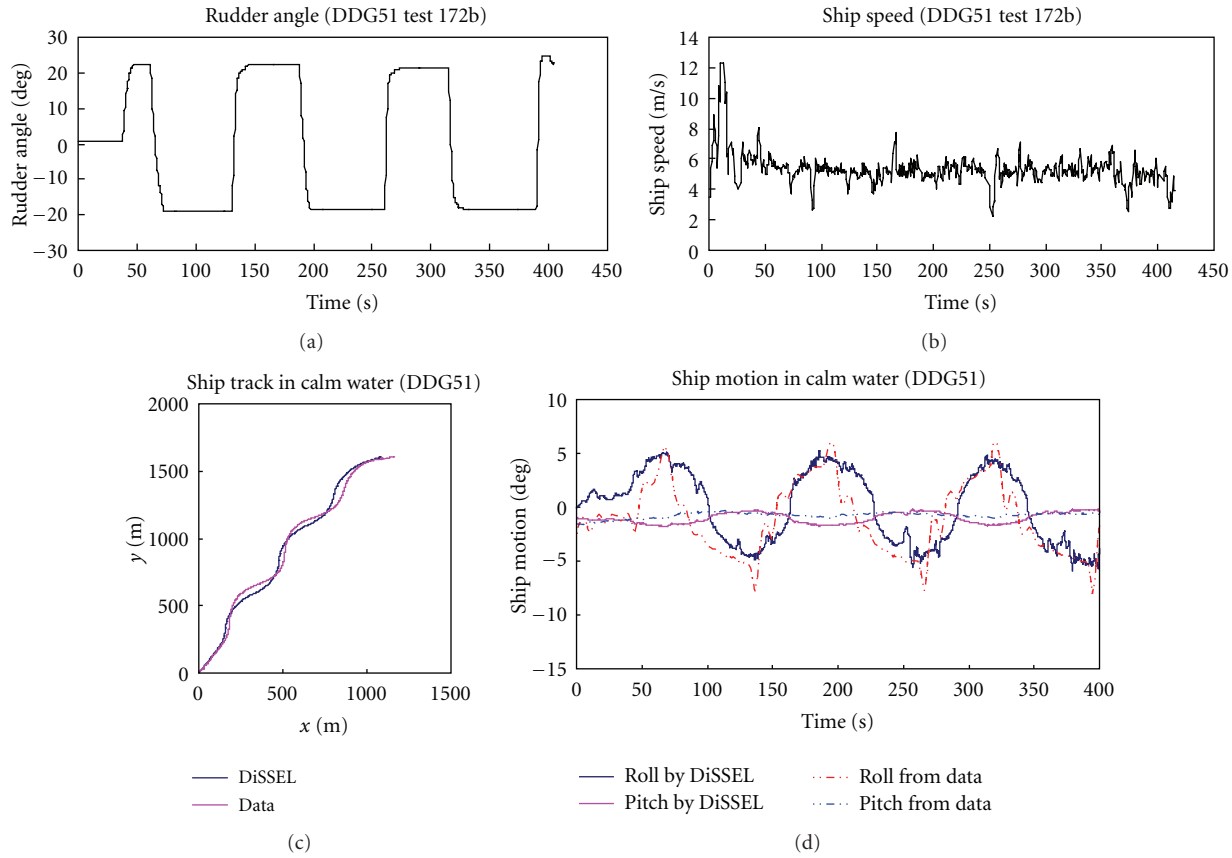

FIGURE 3: Data input for case 3 are shown in (a) and (b). (a) Rudder angle from data in test 172b, (b) ship speed from data in test 172b. Benchmark simulations for case 3 are shown in (c) and (d). (c) Comparison of ship track between simulation and experimental data in test 172b. (d) Comparison of roll and pitch motions between simulations and data in test 172b.

Ae is affected area, and it is a function of object rotational motion angles, wave frequency, nature frequency, and waiting function of wave amplitudes. In the calm water, Ae is only a function of object rotational motion angles and nature frequency.

The separation effect that causes the total hydrodynamic force reduction in the object can be obtained in potential flow:

$$\mathbf{F}_{\text{separation-effect}} = -\iint_{\text{Ae}} \mathbf{n} P_{(s)} ds. \tag{3}$$

The separation effect on the moment in the object is

$$\mathbf{\Gamma}_{\text{separation-effect}} = -\iint_{\text{Ae}} \mathbf{r} \times \mathbf{n} P_{(s)} ds, \tag{4}$$

where $\mathbf{r}$ is rotating arm vector of the object. The "blocking theory" has been well tested with experimental data [16]; it can accurately estimate the bilge keels roll damping, T-foil pitch and roll damping, and lift force for steady turning circles. More details in Lin and Kuang [16].

2.2. Prediction Forces and Moment on Rudder. The effective force and moment on the rudders in the ship coordinate system can be expressed as

$$\begin{aligned}
\mathbf{F}_{\text{rudder}} &= \iint_{\text{A}_0-\text{A}_{0e}} \mathbf{n}_r P_{\text{rudder}}(s) ds \\
&= F_x \mathbf{x}_s + F_y \mathbf{y}_s + F_z \mathbf{z}_s + \mathbf{F}_{\text{coriolis}}, \\
\mathbf{\Gamma}_{\text{rudder}} &= \iint_{\text{A}_0-\text{A}_{0e}} \mathbf{r} \times \mathbf{n}_r P_{\text{rudder}}(s) ds + (\mathbf{x} - \mathbf{x}_C) \times \mathbf{F}_{\text{coriolis}} \\
&= \Gamma_x^r \mathbf{x}_s + \Gamma_x^r \mathbf{y}_s + \Gamma_z^r \mathbf{z}_s + (\mathbf{x} - \mathbf{x}_C) \times \mathbf{F}_{\text{coriolis}},
\end{aligned} \tag{5}$$

where A_0 is total surface area of rudder and A_{0e} is the "affect area" of rudder. The rudder angle, δ, varies with time as specified by the input data, and $\mathbf{\Omega}_\delta$ is the angular velocity of rudder in ship coordinate. $F_z \mathbf{z}_s$ is vertical lift forces on the rudders and $\mathbf{r}$ is rotating arm vector, $\mathbf{x}_s, \mathbf{y}_s, \mathbf{z}_s$ are the three components of unit vectors in the ship-fixed coordinate, $\mathbf{x}_C$ is the position vector of the center of the circle tangent to the point $\mathbf{x}$ on the ship trajectory, and $\mathbf{n}_r$ is rudder surface normal vector. $P_{\text{rudder}}(s)$ is a pressure on the wetted surfaces of the rudder; $\mathbf{F}_{\text{rudder}}$ is force on the rudder, and $\mathbf{F}_{\text{coriolis}}$ is

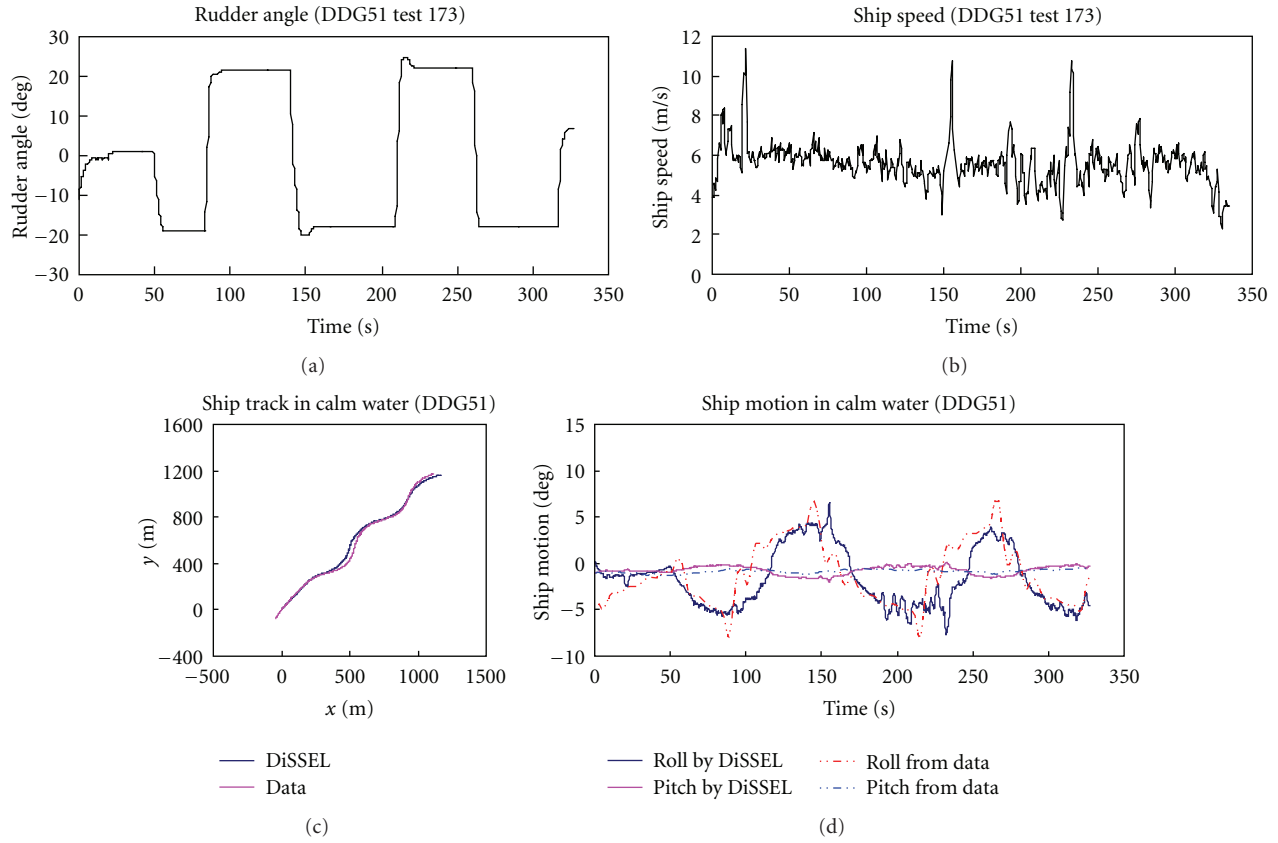

FIGURE 4: The data input for case 4 are shown in (a) and (b). (a) Rudder angle from data in test 173, (b) ship speed from data in test 173. The benchmark simulations for case 4 are shown in (c) and (d). (c) Comparison of ship track between simulations and data in test 173. (d) Comparison of roll and pitch motions between simulations and data in test 173.

the effective Coriolis force due to the rudder angle, δ, which varies in the ship coordinate system and equals

$$\mathbf{F}_{\text{Coriolis}} = \int_{A_0} \rho \left[2\boldsymbol{\Omega}_\delta \times \mathbf{v}_s + \boldsymbol{\Omega}_\delta \times (\boldsymbol{\Omega}_\delta \times \mathbf{x}) + \frac{d\boldsymbol{\Omega}_\delta}{dt} \times \mathbf{x} \right] ds, \quad (6)$$

The effective inflow velocity into the rudder is derived from both the ship forward speed and the accelerated flow in the propeller slipstream. DiSSEL does not have a propeller model, so the velocity into the rudder including the influence of the propeller is empirically defined as

$$u_r = 1.6u_s. \quad (7)$$

$\mathbf{u}_s$ is given ship speed vector. The $1.6u_s$ approximation is a reasonable estimate for naval vessels with Froude numbers between 0.2 and 0.4 for propellers designed for that speed (based on Dr. Young Shen suggestion, 2008). For other types of vessels, the acceleration of the flow by the propeller may be different. In these cases the effective inflow velocity into the rudder should be computed from conservation of momentum based on a user-specified propeller diameter and thrust coefficient.

The yaw moment about the ship center of gravity produced by the rudder is obtained by the appropriate moment arm, r_3,

$$\boldsymbol{\Gamma}_z^r = \iint_{A_0 - A_{0e}} (r_3 \mathbf{x}_s) \times \left(n_y \mathbf{y}_s \right) P_{\text{rudder}}(s) ds, \quad (8)$$

where $r_3 = x_r - x_c$, and n_x, n_y, n_z are the three components of normal vector of rudder surface.

To calculate the forces and moments on the rudders, DiSSEL uses a body exact integration by finite element/finite difference method. After the forces and moments on the rudder are obtained, they are added to the translational and rotational motion equations of the rigid body ship motion in DiSSEL. The calculation of the translation and rotational motion of the ship are discussed in the following section.

2.3. DiSSEL Ship Motion Model. DiSSEL includes two sub-models. The first sub-model is to simulate the ship-wave interaction, which computes the flow around the ship including the influence of the free water surface, the pressure distribution on the ship hull, and the hydrodynamic forces on the ship. The second sub-model is the rigid body motion component, which uses the forces computed by the ship-wave interaction sub-model to predict the six degrees-of-freedom motions of the ship by solving the equations of

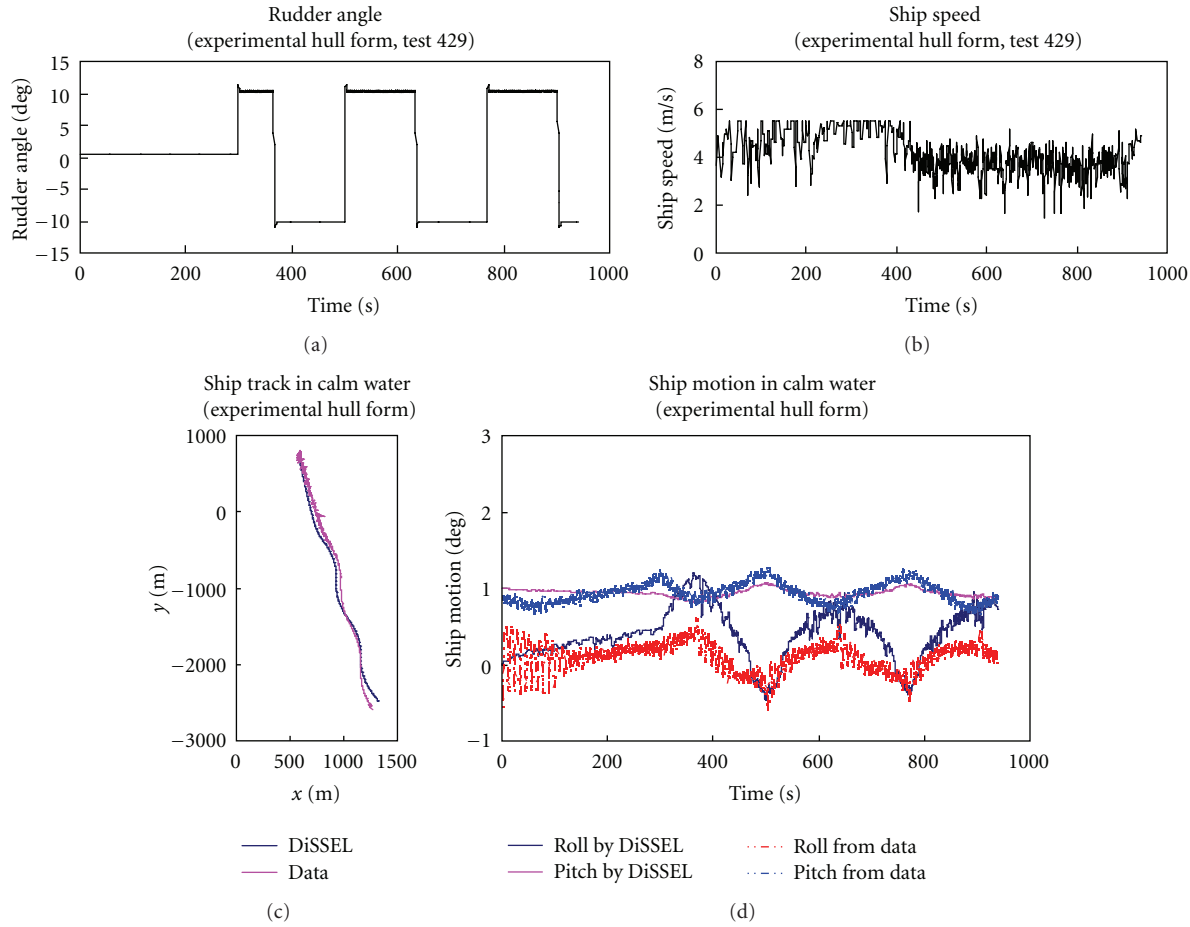

FIGURE 5: The data input for case 5 are shown in (a) and (b). (a) Rudder angle from data in test 429, (b) ship speed from data in test 429. Benchmark simulations for case 5 are shown in (c) and (d). (c) Comparison of ship track between simulation and experimental data in test 429. (d) Comparison of roll and pitch motions between simulation and experimental data in test 429.

motion in the time domain. The rudder force and moment are included as separate forces and moments in the rigid body motion sub-model of the code.

To calculate the forces and moments on the ship hull and all appendages, DiSSEL uses a body exact integration by finite element/finite difference method. In each time step, the waterline based on the ship position and free surface of elevation is defined. Three coordinate systems are used: earth-fixed reference frame, upright ship-fixed reference frame, and ship-fixed coordinate system. Except for the ship track in earth coordinate and incident waves in ship reference frame, all the simulations are in the ship coordinate system. The ship reference frame is defined with its origin on the mean free surface and moves with total horizontal translational velocities.

For the far field, DiSSEL employs the pseudo-spectral method. At each time step, through the ship boundary condition, rigid body motion model gives the ship motion information to the ship-wave interaction model, and the ship-wave interaction model calculated pressure passes back to the rigid body motion model. The finite element/finite difference method exchanges the information with the pseudo-spectral through the collocation points of the pseudo-spectral method. Pseudo-spectral modes and collocation points use a Fast Fourier Transform to exchange information. This method is very accurate and efficient. The convergence speed is $N\log N$ instead of N^2, where N is the number of unknown variables; the details are described in Lin et al. [18]. In the current work, $\mathbf{u}_s$ is ship forward speed and from input data, and $\mathbf{v}_s$ is translational velocity of the ship center of gravity ($\mathbf{v}_h$ is horizontal component vector of translational velocity) and computed by the program at each time step.

Another notice should be made on the definitions of the reference frames used in DiSSEL. In Lin and Kuang [1], two additional reference frames are introduced: the ship reference frame (SRF) and the model reference frame (MRF). The latter is defined to be the reference frame moving horizontally with the ship mass center, but with the origin on the mean free surface. When a ship maneuvers in seaway, its track direction can change. But MRF does not change its orientation. Therefore, the rotational effect from this direction change needs to be accounted for correctly. For details of the reference frames, we refer the reader to Lin and Kuang [1].

2.3.1. Ship Wave Interaction Model. The ship-wave interaction sub-model is computed in a fluid domain of depth H,

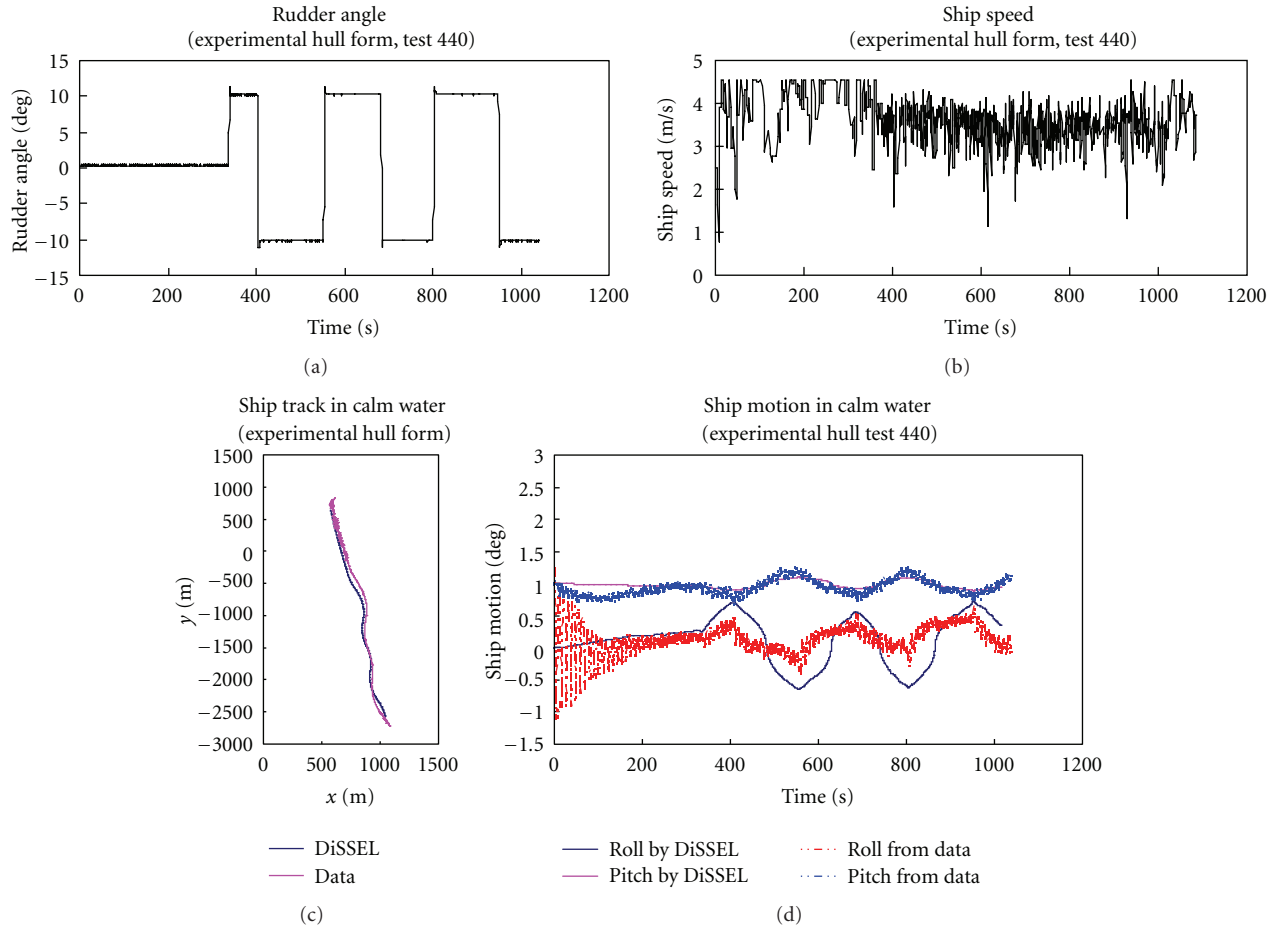

Figure 6: The data input for case 6 are shown in (a) and (b). (a) Rudder angle from data in test 440, (b) ship speed from data in test 440. The benchmarking simulations are shown in (c) and (d). (c) Comparison of ship track between simulation and experimental data in test 440. (d) Comparison of roll and pitch motion between simulation and experimental data in test440.

width D, and length L. Except for the free surface and ocean bottom boundaries, all other boundaries are open, which allows fluid to come in and out through these faces. Such boundaries not only allow the use of a small computational domain, but also increase accuracy.

The fluid is assumed as incompressible,

$$\nabla^2 \varphi \equiv \nabla_h^2 \varphi + \frac{\partial^2 \varphi}{\partial z^2} = 0 \qquad \text{for } -H \le z \le \eta, \tag{9}$$

where φ is velocity potential, η is free surface elevation, and H is water depth.

The dynamic and kinematic boundary conditions at the free surface, $z = \eta$, are

$$\frac{\partial \varphi}{\partial t} + \left(\frac{1}{2}\nabla\varphi + \mathbf{u}_s + \mathbf{v}_h\right)\nabla\varphi + gz + \frac{p}{\rho} + \frac{\partial(\mathbf{u}_s + \mathbf{v}_h)}{\partial t} \cdot \mathbf{x}^* - \nu\nabla_h^2\varphi = 0, \tag{10}$$

$$\frac{\partial \eta}{\partial t} + (\nabla_h \eta) \cdot (\nabla_h \varphi + \mathbf{u}_s + \mathbf{v}_h) = \frac{\partial \varphi}{\partial z}, \tag{11}$$

where $\mathbf{v}_c$ is ship response translational motions and $\mathbf{v}_h$ is its horizontal component (surge and sway), p is the pressure, ρ is the fluid density, ν is the kinematic viscosity, here representing the wave breaking effects, and $\mathbf{x}^*$ is the position vector of a point in space. For a purely potential flow, the viscous dissipation in (10) vanishes. The above equations are solved with the impenetrable boundary conditions at the bottom, $z = -H$,

$$\frac{\partial \varphi}{\partial z} = 0, \tag{12}$$

at the ship hull:

$$\mathbf{n} \cdot (\nabla\varphi + \mathbf{u}_t) = 0, \tag{13}$$

at a point $\mathbf{x}_p$ on the ship hull surface:

$$\mathbf{u}_t = \mathbf{u}_s + \mathbf{v}_c + \mathbf{\Omega} \times \left(\mathbf{x}_p - \mathbf{x}_c\right), \tag{14}$$

where $\mathbf{x}_p$ is the location of a point, p, on the ship surface and $\mathbf{x}_c(x_c, y_c, z_c)$ is the center of gravity in ship-fixed coordinate system. The ship boundary condition is:

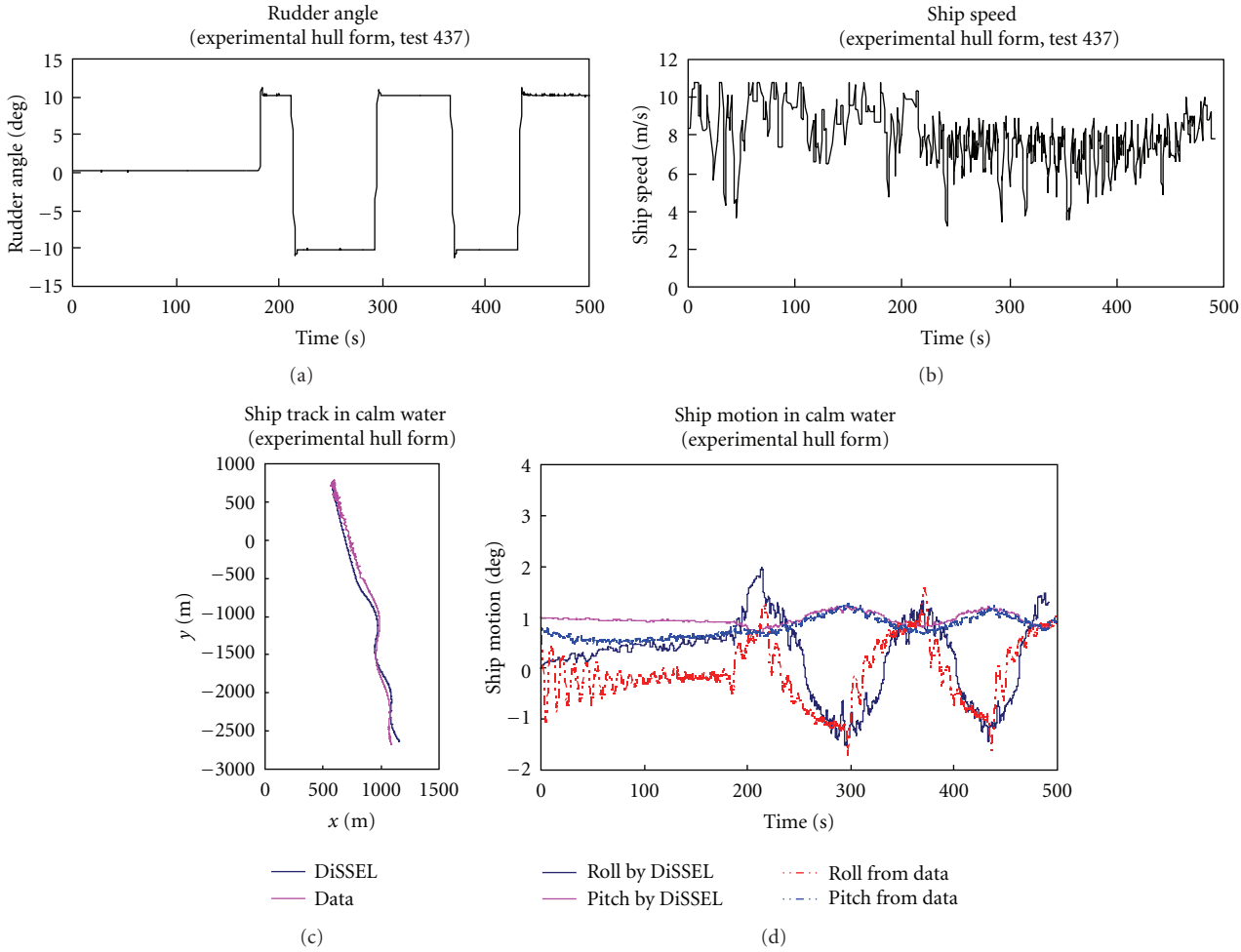

FIGURE 7: The data input for case 7 are shown in (a) and (b). (a) Rudder angle from data in test 437, (b) ship speed from data in test 437 Benchmark simulations for case 7 are shown in (c) and (d). (c) Comparison of roll and pitch motion between the simulation and experimental data in test 437. (d) Comparison of roll and pitch motions between simulation and experimental data in test 437.

2.3.2. Rigid Body Motion Model. In this section, the basic equations of motions for the rigid ship hull are presented. Both the motions and the forces are defined in the ship reference frame with the origin at the ship center of gravity. Positive $\mathbf{x}_s$ is towards the bow, positive $\mathbf{y}_s$ is to port, and positive $\mathbf{z}_s$ is upwards. The origin is at the center of gravity of the ship. Therefore, in the DiSSEL [19] rigid body motion model, the ship translational motion is expressed in MRF by

$$m_{\text{ship}} \frac{d\mathbf{v}_c}{dt} + D_{\text{trans}}\mathbf{v}_c = \mathbf{F}_{\text{ship}} + \mathbf{F}_{\text{rudder}}, \tag{15}$$

where m_{ship} is total ship mass, $\mathbf{F}_{\text{ship}}$ includes the buoyancy restoring forces, $\mathbf{F}^g_{\text{ship}}$, and the hydrodynamic pressure forces, $\mathbf{F}^p_{\text{ship}}$, on the ship hull, and D_{trans} is the dissipation of translation motion due to wave breaking. The surge, sway, and heave can be obtained in (15).

The rigid body rotation is governed by the Liouville Equation defined in the ship reference frame:

$$\mathbf{I} \cdot \frac{d\boldsymbol{\Omega}}{dt} + \boldsymbol{\Omega} \times (\mathbf{I} \cdot \boldsymbol{\Omega}) + D_{\text{rotat}}\boldsymbol{\Omega} = \boldsymbol{\Gamma}_{\text{ship}} + \boldsymbol{\Gamma}_{\text{rudder}} + \boldsymbol{\Gamma}_{c(1)}, \tag{16}$$

where $\mathbf{I}$ is the mass moments inertia vector about the ship center of gravity, $I_{(i,i)}$ is the moments of inertia about the ship center of gravity in ith direction, $\boldsymbol{\Omega}$ is rotational response angular velocity vector (roll, pitch, and yaw). $\boldsymbol{\Gamma}_{\text{ship}}$ is the moment on the ship, and it includes the buoyancy restoring moment, $\boldsymbol{\Gamma}^g_{\text{ship}}$, and the hydrodynamic pressure moment, $\boldsymbol{\Gamma}^p_{\text{ship}}$, on the ship hull and roll moment $\boldsymbol{\Gamma}_{c(1)}$, due to the direction of ship speed change, and D_{rotat} is the dissipation of rotational motion due to the wave breaking and bilge keels. The ship forces $\mathbf{F}^p_{\text{ship}}$ and moment $\boldsymbol{\Gamma}^p_{\text{ship}}$ are calculated by integrating the pressure and pressure multiplied by the lever arm over the ship wetted surface in the normal vector coordinate, respectively. The details are in [18–20].

An additional roll moment acts on the ship as a result of its turning motion. This additional roll moment about the ship center of gravity can be computed as

$$\begin{aligned}\boldsymbol{\Gamma}_{c(1)} &= \iint_s m_{\text{ship}} r_1 \frac{(u_s + dX_1/dt)^2 + (dX_2/dt)^2}{R} ds \\ &\approx \iint_s m_{\text{ship}} r_1 \frac{(u_s + dX_1/dt)^2 + (dX_2/dt)^2}{\sqrt{(u_s + dX_1/dt)^2 + (dX_2/dt)^2}/(d\theta^*/dt)} ds, \\ &= \iint_s m_{\text{ship}} r_1 \sqrt{(u_s + dX_1/dt)^2 + (dX_2/dt)^2}(d\theta^*/dt) ds,\end{aligned} \tag{17}$$

where X_1 and X_2 are the ship moving distances due to surge and sway motions, respectively. R is turning radius and the roll moment arm is

$$r_1 = \left[\left(\mathbf{x}_p - \mathbf{x}_c\right) \times \mathbf{n}\right] \cdot \mathbf{x}, \tag{18}$$

where $\mathbf{x}_p$ is the location point of ship surface. Roll, pitch and yaw moments can be obtained by (16) and (17). The drift angle, β, is the angle in the horizontal plane between ship's latitude and the ship's longitudinal axis. The drift angle is computed:

$$\beta = \tan^{-1} \frac{v_2}{u_s + v_1}. \tag{19}$$

The "total heading angle," θ^*, is

$$\theta^* = \theta_3 + \beta, \tag{20}$$

where θ is rotational angle vector of the ship and θ_i is a rotational angle of the ship in ith direction. The track of the ship in the earth-fixed coordinate system is defined as

$$\mathbf{x}_{\text{track}} = x_{\text{track}}\hat{\mathbf{x}} + y_{\text{track}}\hat{\mathbf{y}}, \tag{21}$$

where $\hat{\mathbf{x}}, \hat{\mathbf{y}}, \hat{\mathbf{z}}$ are the vectors in the earth-fixed coordinate system, and the track is computed at each time step with the following equation:

$$\begin{aligned}x_{\text{track}(i\text{step})} &= x_{\text{track}(i\text{step}-1)} + X_{1(i\text{step})} \\ &\quad + \left[\left(u_{s(i\text{step})} + \frac{dX_1}{dt}\right)\cos\left(\theta_{3(i\text{step})}\right) \right. \\ &\quad \left. - \frac{dX_2}{dt}\sin\left(\theta_{3(i\text{step})}\right)\right] dt_{(i\text{step})}, \\ y_{\text{track}(i\text{step})} &= y_{\text{track}(i\text{step}-1)} + X_{2(i\text{step})} \\ &\quad + \left[\left(u_{s(i\text{step})} + \frac{dX_1}{dt}\right)\sin\left(\theta_{3(i\text{step})}\right) \right. \\ &\quad \left. + \frac{dX_2}{dt}\cos\left(\theta_{3(i\text{step})}\right)\right] dt_{(i\text{step})}.\end{aligned} \tag{22}$$

3. Benchmarking

In [1], we have benchmarked the predicted surge and sway forces, and yaw moment, as well as the forces derived from the surge, sway, and yaw motions with experimental data of Pre-Contract DDG51 for steady turning circles in calm water. In the steady turning circles in calm water, only the surge, sway, yaw, and heel motions are significant. However, for unsteady maneuvering cases, even in calm water, all six degrees-of-freedom motions are significant. Therefore, in this study we will focus on the comparison of the predicted ship motions (surge, sway, yaw, roll, and pitch motions) with experimental data. Heave motion will not be shown because heave was not measured experimentally. The coupled computational system presented in this study is fully nonlinear. The six degrees-of-freedom ship motions interact with each other. If the benchmarking shows that the predicted five degrees-of-freedom ship motions (excepting heave motion) agree well with the experimental data, then the predicted heave motion will also agree with the experimental data because the heave motion is strongly linked to pitch motion. The benchmark comparison includes the Pre-Contract DDG51 and the Experimental Hull Form. The ship characteristics of Pre-Contract DDG51 have been described in [1], the Experimental Hull Form is a proprietary hull form, and we are unable to discuss its characteristics. In the following comparisons, four cases for each ship hull are randomly chosen. The time series of rudder angle and ship forward speed are the input data to the simulation and are shown in the figures as (a) and (b), respectively, of each case. The comparison for the ship track, roll and pitch motions between the simulations results and data are shown in the figures as (c) and (d), respectively, for each case.

3.1. Pre-Contract DDG51. In this subsection, we compare the simulation results with experimental data for DDG51. The input data is time series of rudder angle and ship forward speed and output is six degrees-of-freedom ship motions. We have benchmarked all test cases, but in the following, we randomly choose four cases to show (Figures 1, 2, 3, and 4). All four cases showed that the simulation of ship motions (surge, sway, roll, pitch, and yaw motions) has very good agreement with experimental data for Pre-Contract DDG51. The good agreement in surge, sway, and yaw can be observed in the ship track. There is not any heave motion data in these tests; therefore, we cannot benchmark the heave motion of simulations. However, six degrees-of-freedom motions are interacting each other, especially pitch and heave, if five degree-of-freedom ship motions are accurately predicted, then the heave motion should be accurately predicted as well.

3.2. Experimental Hull Form. In order to test the universal fully-nonlinear prediction capabilities, we will compare simulated and experimental ship motion data for a different ship hull. To study the different ship hull, we have not changed any parameters in the computational system, except the ship and rudder characteristic (ship mass, ship length, ship profile, rudder area, etc), and time series of rudder angle and ship forward speed. For experimental hull form, we randomly choose four cases as showed in Figures 5, 6, 7, and 8. The measured ship speeds for both the Pre-Contract DDG51 and the Experimental Hull Form were obtained by differentiating the x-y track time history with respect to time. The ship speeds obtained for the Pre-Contract DDG51 showed some higher frequency fluctuations, which

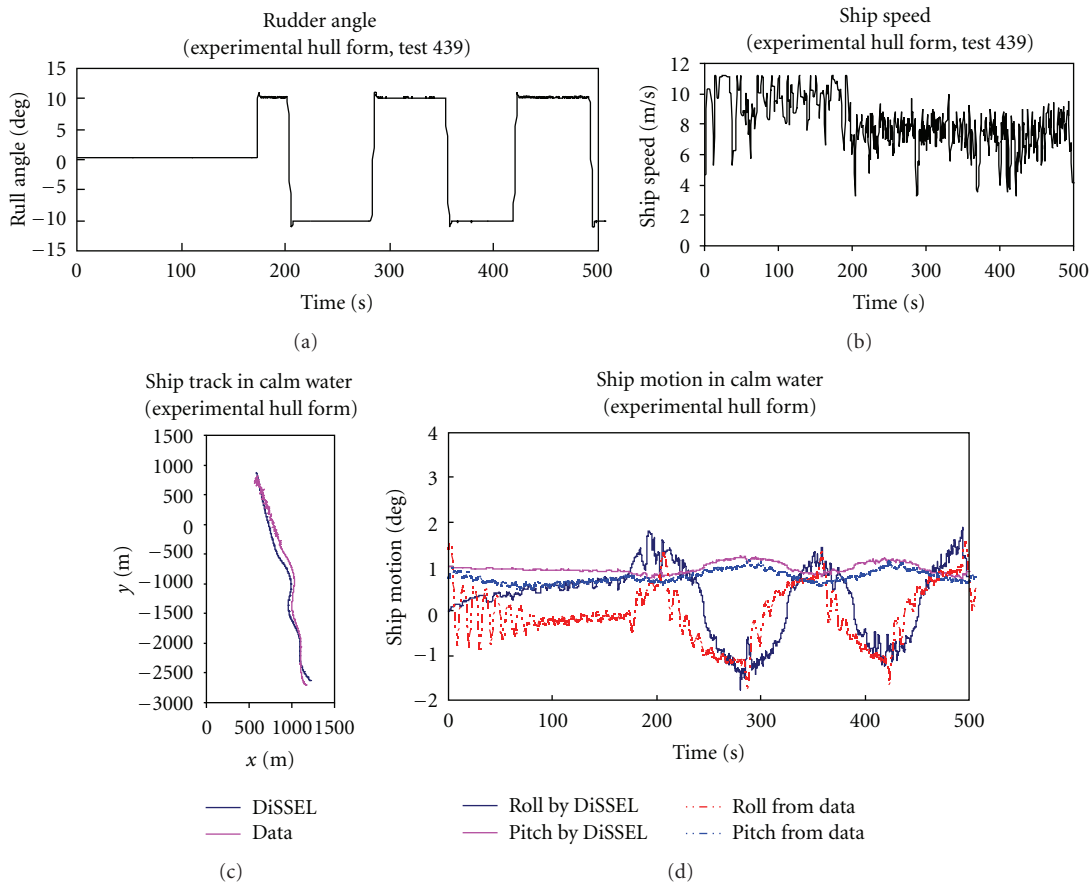

FIGURE 8: The data input for case 8 are shown in (a) and (b). (a) Rudder angle from data in test 439, (b) ship speed from data in test 439. Benchmark simulations for case 8 are shown in (c) and (d). (c) Comparison of ship track between simulation and experimental data in test 439. (d) Comparison of roll and pitch motion between simulation and experimental data in test 439.

may be real or a result of measurement errors in the tracker. For the Pre-Contract DDG51, the original unfiltered speed data were used. However, the measured ship speeds for the Experimental Hull Form showed larger and unrealistic fluctuations; for example, many large speeds are far over maximum ship speed. Therefore, in this section, we make some corrections to the measured ship speed, by taking the running average of the speed over a period of 60 seconds.

The comparison of ship motions between numerical simulations and experimental data for the experimental hull form are as good as those for Pre-Contract DDG51 in all the cases, because the new method is self-consistent and the numerical solutions satisfy the original equations and boundary conditions.

4. Conclusion

A physics-based and self consistent, fully-nonlinear computational system for predicting ship steering capabilities as well as the six degrees-of-freedom ship motions has been presented. The six degrees-of-freedom ship motions and their interactions are calculated from the original equations and boundary conditions; no other empirical parameters are involved, except an empirical function that is used for the influence of the propeller slipstream on the rudder, which is included using a flow acceleration factor. The numerical simulations of ship motions (heave motions are not shown because there is no experimental data) for two entirely different ship hulls by the new method agree reasonably well with the experimental data when ships unsteadily maneuver in calm water.

Acknowledgments

The authors wish to thank Mr. Terry Applebee, Head of the Seakeeping Division, NSWCCD, for his many useful comments and suggestions. They also want to thank the Seakeeping Division at NSWCCD for providing the experimental data used for the correlation shown in this paper. Finally they want to thank Dr. Young T. Shen for his many useful suggestions. This work is supported by Naval Surface Warfare Center Independent Laboratory In-House Research (ILIR) program administrated by Dr. John Barkyoumb.

References

[1] R. Q. Lin, M. Hughes, and T. Smith, "Prediction of ship steering capabilities with a fully nonlinear ship motion model. Part

1: maneuvering in calm water," *Journal of Marine Science and Technology*, vol. 15, no. 2, pp. 131–142, 2010.

[2] R.-Q. Lin and W. Kuang, "A fully nonlinear, dynamically consistent numerical model for ship maneuvering in a seaway," *Modeling and Simulation in Engineer*, vol. 2011, Article ID 356741, 10 pages, 2011.

[3] S. W. Chau, "Computation of rudder force and moment in uniform flow," *Ship Technology Research*, vol. 45, no. 1, pp. 3–13, 1998.

[4] O. M. El Moctar, "Numerical determination of rudder forces," Euromech 374, Poities, 1998.

[5] J.-T. Lee, "A potential based panel method for the analysis of marine propellers in steady flow," Tech. Rep. 87-13, Department of Ocean Engineering, MIT, 1988.

[6] M. Tamashima, S. Matsui, J. Yang, K. Mori, and R. Yamazaki, "The method for predicting the performance of propeller-rudder system with rudder angles and its application to rudder design," *Transaction of the West-Japan Society of Naval Architects*, vol. 86, pp. 53–76, 1993.

[7] J. M. Han, D. S. Kong, I. H. Song, and C. S. Lee, "Analysis of the cavitating flow around the horn-type rudder in the race of propeller," in *Proceedings of the 4th International Symposium on Cavitation*, pp. 20–23, California Institute of Technology, Pasadena, Calif, USA, June 2001.

[8] S. A. Kinnas, H. Lee, H. Gu, and S. Natarajan, "Prediction of sheet cavitation on a rudder subject to propeller flow," *Journal of Ship Research*, vol. 51, no. 1, pp. 65–75, 2007.

[9] J. P. Hacket, C. O. E. Burgh, and W. H. Brewer, "Manufacturing tolerance effects on ship rudder force/cavitation performance," in *Proceedings of the SNAME Marine Technology Conference and Expo and Ship Production Symposium*, Houston, Tex, USA, October 2005.

[10] A. C. Hochbaum, F. Stern, K. Agdrup et al., "Final Report and Recommendations to 25th ITTC," in *Proceedings of the 25th International Towing Tank Conference (ITTC '08)*, vol. I, pp. 143–208, Fukuoka, Japan, September 2008.

[11] H. Söding, "Limits of potential theory in rudder flow predictions," in *Proceedings of the 22nd Symposium on Naval Hydrodynamics*, Weinblum Lecture, pp. 622–637, Washington, DC, USA, 1999.

[12] M. Altosloe, M. Figari, and M. Viviani, "6DOF simulation of maneuvering and propulsive performance of waterjet propelled Mega Yacht," Fast2009, Athens, Greece, 2009.

[13] R. Kimoto, T. Katayama, and Y. Ikeda, "Effects of running attitude on hydrodynamic forces for oblique towed planing craft," in *Proceedings of the 2nd Asia-Pacific Workshop on Hydrodynamics (APHydro '04)*, pp. 115–122, Busan, Korea, 2004.

[14] T. Katayama, R. Kimoto, and Y. Ikeda, "Effects of running attitudes on maneuvering hydrodynamic forces for planing hull," in *Proceedings of the International Conference on Fast Sea Transportation (FAST '05)*, Petersburg, Russia, 2005.

[15] T. Katayama, T. Taniguchi, H. Fujii, and Y. Ikeda, "Development of maneuvering simulation method for high speed craft using hydrodynamic forces obtained from model tests," Fast2009, Athens, Greece, 2009.

[16] R. Q. Lin and W. Kuang, "Modeling nonlinear roll damping with a self-consistent, strongly nonlinear ship motion model," *Journal of Marine Science and Technology*, vol. 13, no. 2, pp. 127–137, 2008.

[17] L. D. Landau and E. M. Lifshitz, *Fluid Mechanics*, Pergamon Press, Oxford, UK, 1987.

[18] R. Q. Lin, W. Kuang, and A. M. Reed, "Numerical modeling of nonlinear interactions between ships and surface gravity waves, part 1: Ship waves in calm water," *Journal of Ship Research*, vol. 49, no. 1, pp. 1–11, 2005.

[19] R.-Q. Lin and W. Kuang, "A fully nonlinear, dynamically consistent numerical model for solid-body ship motion. I. Ship motion with fixed heading," *Proceeding of Royal Society A*, vol. 467, no. 2128, pp. 911–927, 2011.

[20] R.-Q. Lin and W. Kuang, "Numerical modeling of nonlinear interactions between ships and surface gravity waves II: ship boundary condition," *Journal of Ship Research*, vol. 50, no. 2, pp. 181–186, 2006.